applied sciences

MDPI

*Article*

# The Isothermal Oxidation of High-Purity Aluminum at High Temperature

**Eric N. Coker [1], Burl Donaldson [1], Walter Gill [1], Nadir Yilmaz [2] and Francisco M. Vigil [3,*]**

[1] Sandia National Laboratories, Albuquerque, NM 87123, USA
[2] Department of Mechanical Engineering, Howard University, Washington, DC 20059, USA
[3] Los Alamos National Laboratory, Los Alamos, NM 87545, USA
* Correspondence: franciscov@lanl.gov

**Abstract:** The isothermal oxidation in air of high purity aluminum sheet was studied as a function of temperature using Thermogravimetric Analysis simultaneously with Differential Scanning Calorimetry (TGA/DSC). The rates and extents of oxidation were found to be non-linear functions of the temperature, in agreement with the literature. Between 650 °C and 750 °C very little oxidation took place; at 850 °C oxidation occurred after an induction period, while at 950 °C oxidation occurred without an induction period. At oxidation temperatures between 1050 °C and 1150 °C rapid passivation of the surface of the aluminum occurred, while at 1250 °C and above, an initial rapid mass increase was observed, followed by a more gradual increase in mass. The initial rapid increase in mass was accompanied by a significant exotherm, which was quantified by DSC. At temperatures of 1050 °C and above the specimen coalesced into a spheroidal particle, whereas at lower temperatures the original morphology was retained due to the cohesive strength of the native oxide layer. Cross-sections of oxidized specimens were characterized by scanning electron microscopy (SEM); the observed alumina skin thicknesses correlated qualitatively with the observed mass increases. Interrogation of the surface of an oxidized spheroidal particle by SEM showed a fractured alumina shell around a partially hollow core of aluminum which appeared to have grain boundaries.

**Keywords:** isothermal oxidation; high-purity aluminum; high temperature; energetics

check for updates

**Citation:** Coker, E.N.; Donaldson, B.; Gill, W.; Yilmaz, N.; Vigil, F.M. The Isothermal Oxidation of High-Purity Aluminum at High Temperature. *Appl. Sci.* **2023**, *13*, 229. https://doi.org/10.3390/app13010229

Academic Editor: Juan García Rodríguez

Received: 22 November 2022
Revised: 14 December 2022
Accepted: 21 December 2022
Published: 24 December 2022

**Copyright:** © 2022 by the authors. Licensee MDPI, Basel, Switzerland. This article is an open access article distributed under the terms and conditions of the Creative Commons Attribution (CC BY) license (https://creativecommons.org/licenses/by/4.0/).

## 1. Introduction

A considerable body of work exists describing the oxidation or ignition of aluminum particles at elevated temperature. Aluminum particle behavior in an open atmosphere propellant burn has been investigated in detail [1–3]. For nominal rocket motor pressures, the aluminum particles oxidize to aluminum oxide in the gas phase and liberate significant combustion energy which also minimizes combustor instability. However, for low or atmospheric pressure combustion, which would be expected during rocket abort or launch pad malfunction, the outcome is not clear. Characterization of the thermal-chemical-physical environment in and around a plume formed from a burning fragment of solid rocket fuel at atmospheric pressure would aid in efforts to model accident scenarios. Ejected burning fragments of solid rocket fuel were observed in prior accident scenarios, such as the Titan 34D-9 accident in 1986 which contained 421,569 kg of solid propellant [4]. Burning propellant fragments pose a hazard to first responders and lead to the unintended ignition of nearby fuel sources.

The particulate sources, while being representative of commercial products, suffer from broad particle size ranges (hence varying surface areas), varying levels of impurities, and being subjected to dynamic heating; all of which can lead to uncertainties in results that potentially could confound general interpretation. To address this issue, we put forth a single heating experiment that is used to explore and confirm the accepted behavior of aluminum surfaces exposed to high temperature air environments. To gain a clearer scientific understanding of the processes involved in the air-oxidation of aluminum, high purity,

low specific surface area sheet was used in the present study. An additional level of control used in the current work (but absent in most previously published work) was to initiate oxidation once the specimen had stabilized at the desired oxidation temperature, i.e., the initial heat-up and stabilization was carried out under high purity inert gas stream.

In general, the oxidation of aluminum in air can be described as occurring in four distinct stages. Trunov et al. [5] illustrated these oxidation stages clearly, and in situ X-ray diffraction has been used to monitor the phase changes occurring in the $Al/Al_2O_3$ system during heat treatment in air [6]. During aluminum combustion, an oxide layer may quickly grow on an aluminum surface which is exposed to an oxidizer. The thickness of the alumina shell depends on several factors including exposure time, temperature and the oxidizer. Oxide layer formation, grain orientation and other physical elements affect aluminum deformation at high temperature [7,8].

The native amorphous alumina layer covering a particle of aluminum (present even at room temperature) initially grows extremely slowly during the low temperature oxidation stage I, which extends up to about 550 °C. The rate of this process is believed to be controlled by the outward diffusion of aluminum cations [9]. The amorphous oxide remains stable, due to the energy of the oxide–metal interface, only up to a critical thickness of about 5 nm [10,11]. The amorphous oxide transforms into γ-alumina once the critical thickness is approached or when the temperature becomes sufficiently high. Since the density of γ-alumina is greater than that of amorphous alumina [12], and the smallest γ-alumina crystallites have a size of about 5 nm [13], if the thickness of the amorphous layer was less than 5 nm, the newly formed γ-alumina crystallites are no longer able to form a continuous layer covering the aluminum surface. Consequently, the beginning of stage II (ca. 550 °C) is accompanied by an increase in the rate of oxidation, and as the openings in the oxide coating heal, the rate of oxidation decreases. By the end of stage II at around 650 °C, a polycrystalline layer of γ-alumina has formed that covers the entire surface of the aluminum. During stage III (approximately 650 °C–1050 °C) the growth of γ-alumina continues at a rate which is limited by the inward diffusion of oxygen anions along grain boundaries [9,14]. Growth of the γ-alumina layer can be accompanied by phase transformations into other transition polymorphs, such as δ-alumina and θ-alumina. Due to the similarity in density of these polymorphs with γ-alumina [12], such transitions are not expected to affect the oxidation rate significantly. At sufficiently high temperature the transition alumina polymorphs become destabilized, and begin to convert to α-alumina, indicating the end of Stage III. When the first α-alumina crystallites begin to form at the end of stage III, the thickness of the γ-alumina layer decreases due to the greater density of the α-alumina phase (a volume contraction of 13.8% is expected on converting γ-alumina to α-alumina), and the oxidation rate increases momentarily [15]. Stage IV is considered to start when the oxide scale is completely transformed to α-alumina, at about 1050 °C. Once most of the oxide layer is transformed to coarse and dense α-alumina crystallites resulting in continuous polycrystalline coverage, grain boundary diffusion slows down, and the oxidation rate decreases rapidly.

One significant difference between the present and most of the earlier work is that in the present work, the temperature range for stage I (growth of amorphous oxide layer) was traversed without exposure of the sample to an oxidizing environment; air was introduced in one of the later stages. The oxidation of molten aluminum was studied by Bergsmark et al. [16]. In addition, there are a number of investigations in literature in relation to oxidation kinetics and behavior of aluminum alloys [17–21].

The present work is not intended to contradict, or expand on previous studies of aluminum oxidation, but is intended be more of a phenomenological objective, and selecting the isothermal test conditions provides useful information. More specifically, the ignition of aluminum particles is known to be directly influenced by the strength of the oxide barrier which forms on the particle exterior. Additionally, the thickness and mechanical integrity of the barrier is directly influenced by the conditions under which it forms. Hence, the isothermal testing protocol provides known initial conditions and the start of the

experiment will be the beginning of air exposure after the sample has been brought to the stated initial temperature. Hence, in summary, how the barrier influences particle ignition is the ultimate application of this study but extending the current study to particle ignition is a separate topic. Insight into how the barrier influences particle ignition will contribute to the development of a model that quantifies the risk associated with a launch pad abort or accident involving solid fueled rocket motors and high hazard payloads.

## 2. Experimental Methods

The aluminum was obtained from Johnson Matthey, and had a purity of 99.998% and a thickness of 0.5 mm. A steel punch was used to cut out circular specimens with a diameter of ~4.9 mm from the aluminum sheet. The circular specimens fit snugly into the bottom of high-purity alumina crucibles, and had a mass of about 26 mg. The specimens were characterized under inert atmosphere (UHP argon) and oxidizing atmosphere (75% ultra-zero air—25% UHP argon) with TGA/DSC (STA 449-F3 Jupiter, Netzsch Instruments, Selb, Germany) during heating under argon to a pre-determined temperature and oxidizing at that temperature for a set amount of time. Total gas flow rates were maintained at 160 sccm throughout each experiment. In all experiments, a heating rate of 20 °C/min was used from ambient to 600 °C, and from 700 °C to the final oxidation temperature. In the range 600 °C to 700 °C a rate of 5 °C/min was used to enable accurate monitoring of the aluminum melting temperature (660.3 °C; used as an internal temperature standard). For the experiment in which oxidation occurred at 650 °C, the sample was first heated to 700 °C then cooled down to 650 °C. In all experiments, the specimen was heated under inert atmosphere to the desired oxidation temperature, and was allowed to stabilize at that temperature under flowing inert gas for 15 min prior to initiating air flow.

All TGA/DSC data have been corrected by baseline subtraction. In order to do this, blank experiments (empty crucibles) were run under exactly the same conditions as the experimental runs, and the blank data was then subtracted from the experimental data. Prior to starting each TGA/DSC experiment, the instrument was evacuated and back-filled with argon three times, then allowed to sit idle under the gas flow conditions to be used in the experiment for at least 15 min to ensure a clean, consistent atmosphere and stable balance reading and DSC signal at the start of each run.

Scanning Electron Microscope (SEM) images were acquired using a JEOL JXA-5900LV, with a Noran System 7 EDS (JEOL USA, Inc., Peabody, MA, USA). Metallographic specimens were cold mounted in epoxy resin, ground, polished, and etched using Barker's reagent (200 mL distilled $H_2O$ and 4 mL $HBF_4$). An electrolytic etch was utilized at 20 Volts for ~40–80 s. Specimens that were not used as metallographic samples were imaged without potting to observe surface features.

## 3. Results and Discussion

### *3.1. Thermogravimetric Analysis—Differential Scanning Calorimetry*

TGA and DSC results are shown in Figures 1 and 2, respectively. The TGA data in Figure 1 shows the oxidation behavior versus time during isothermal holds at temperatures between 650 °C and 1550 °C. Time zero is defined as the point at which air was first introduced into the TGA, and the data plotted begins 10 min before $t = 0$. The observed behavior (i.e., oxidation mass change versus temperature of exposure to air) is directly comparable to previous literature reports where aluminum samples were heated at various rates under oxidizing conditions, described in the introduction. One significant difference between the present and most of the earlier work is that in the present work, the temperature range for stage I (growth of amorphous oxide layer) was traversed without exposure of the sample to an oxidizing environment; air was introduced in one of the later stages, using the definitions given in the introduction.

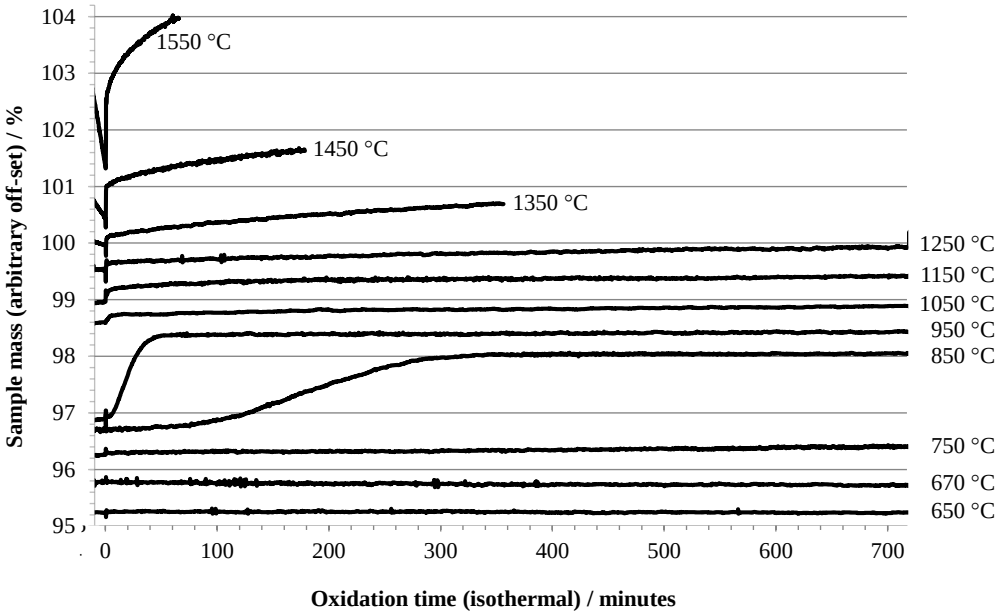



**Figure 1.** TGA results for 0.5 mm aluminum heated under argon to the indicated temperature, then exposed to air (at $t = 0$).

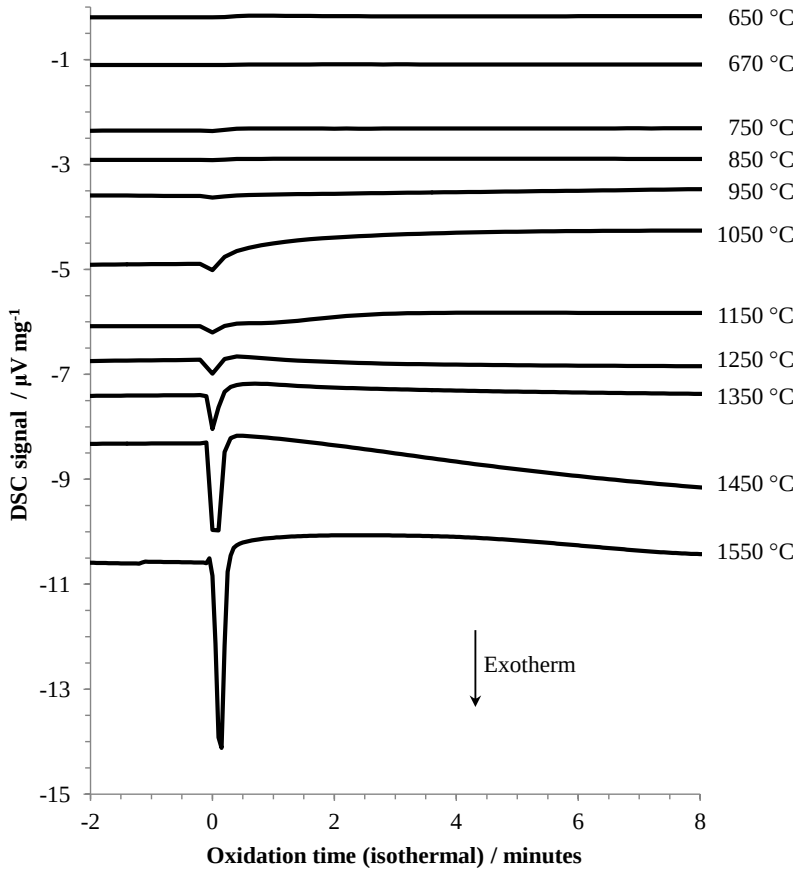



**Figure 2.** DSC results for aluminum heated under argon to the indicated temperature, then exposed to air (at $t = 0$).

The TGA data recorded during oxidation at 650 °C and 670 °C showed negligible mass increase during a 12 h hold (Figure 1). At an oxidation isotherm of 750 °C, the onset of slow oxidation was observed, while at 850 °C a gradual mass increase occurred with

a rate that initially accelerated and became significant after about 1 hr of exposure to air. A similar induction period was reported by Bergsmark et al., for commercial grade aluminum (>1500 ppm impurity level) at 850 °C under pure oxygen [16]. Kolarik et al. [6] observed the delayed transformation of γ-alumina to α-alumina by in situ XRD after holding for 160 min in air at 850 °C. At 950 °C a similar overall mass increase was seen, but at a more rapid rate and without a significant induction period. The observations of TGA data in this temperature range are consistent with stage III oxidation. The induction period seen at 850 °C may be a consequence of the necessity to build up a contiguous layer of γ-alumina on the specimen prior to transition to δ-, θ-, and eventually α-polymorphs, and that the buildup of γ-alumina is slow at 850 °C.

The slow, but gradually increasing (with temperature) oxidation at 1050 °C, 1150 °C, and 1250 °C coincides with the transition from stage III into stage IV oxidation. At 1350 °C and above, the rate of oxidation becomes increasingly significant. Two other factors are apparent at the highest oxidation temperatures, (1) the sample mass decreases during the isothermal hold before air is admitted, and (2) there is a large, almost instantaneous increase in mass upon initial exposure to air, followed by a more gradual increase. This rapid increase in mass is accompanied by a significant exotherm, as shown in Figure 2. At oxidation temperatures below 1050 °C the exotherm was barely noticeable.

Figure 3 plots the energy released during the initial rapid oxidation event, based upon the measured peak intensity (area) for each exotherm, against oxidation temperature. The decreasing mass prior to oxidation at the highest temperatures is ascribed to vaporization of aluminum.

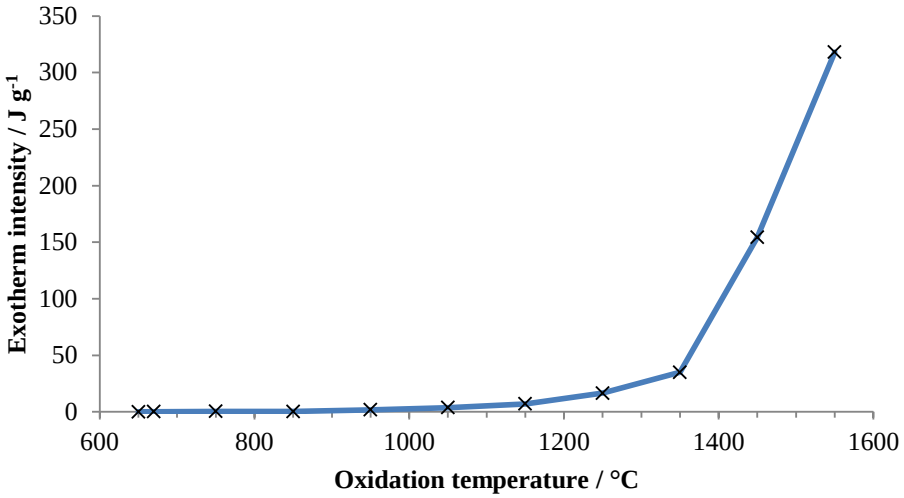



**Figure 3.** Energy released upon first exposure ofaluminum to air versus temperature of exposure. Energy is normalized to the total specimen mass at the beginning of the experiment.

Figure 4 shows an expansion of the region around the introduction of air for experiments conducted at oxidation temperatures of 1350 °C, 1450 °C, and 1550 °C. It can be seen that vaporization becomes noticeable slightly below 1350 °C, and the rate increases rapidly with temperature.

The rates of mass loss seen in Figure 4 were calculated for the linear portions of the mass change curves during evaporation of aluminum, and these are plotted in Figure 5 together with data for the vapor pressure of aluminum at similar temperatures. Not surprisingly, there is good correlation between the trend of rate of mass loss due to evaporation of aluminum and the reported vapor pressures. The mass loss rate and vapor pressure increase approximately exponentially with temperature.

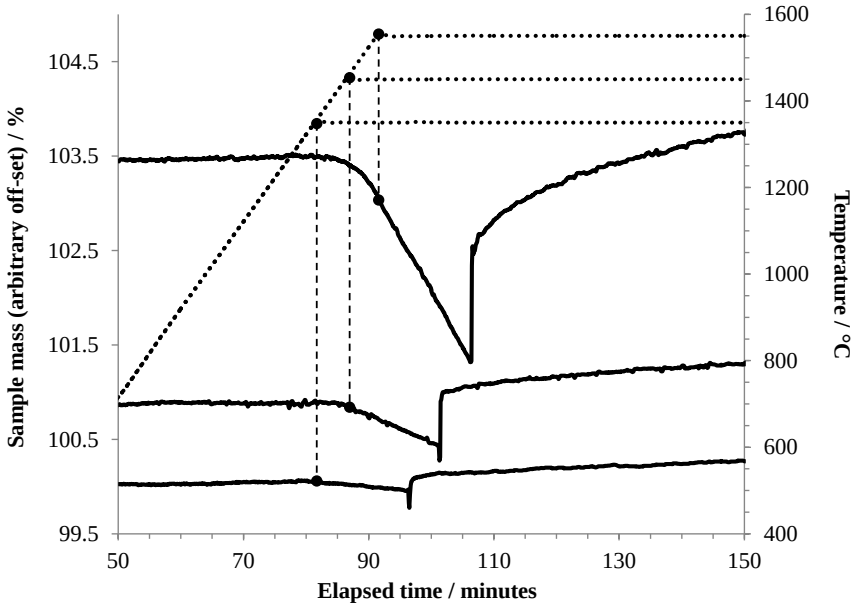



**Figure 4.** TGA results foraluminum heated to 1350 °C or higher under argon, held at that temperature for 15 min, then exposed to air. The vertical dashed lines tie the respective TGA curves to the point on the temperature curve (dotted line) where the isothermal hold began. In this plot, the beginning of each experiment is taken as $t = 0$. The point at which air flow began is recognized by the sudden mass increase in each curve.

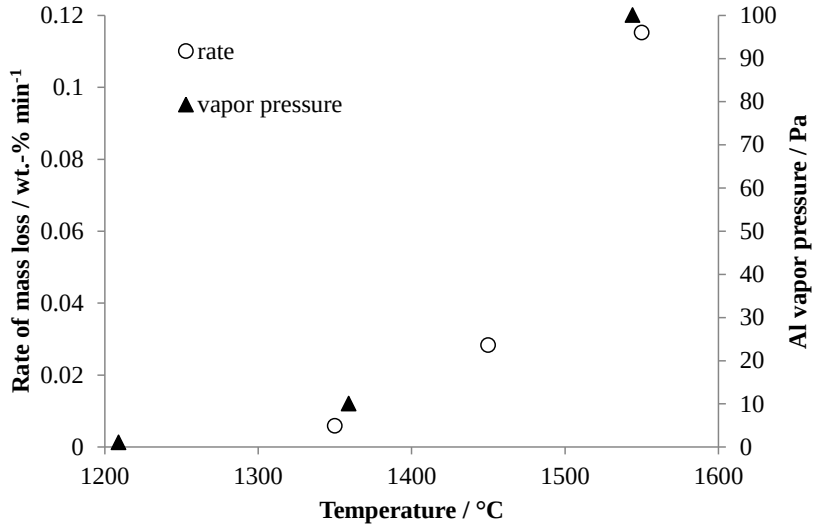



**Figure 5.** Rates of mass loss duringaluminum evaporation taken from Figure 4 compared to the published vapor pressure ofaluminum at similar temperatures. Thealuminum vapor pressure data was taken from http://www.knowledgedoor.com/2/elements_handbook/vapor_pressure.html (accessed on 28 April 2017).

### *3.2. Scanning Electron Microscopy*

Samples of aluminum which had been oxidized at temperatures between 750 °C and 1550 °C were potted in epoxy resin and sectioned with a diamond saw to reveal cross-sections of the specimens. These were then imaged in a scanning electron microscope. Representative images depicting the alumina shell that formed upon oxidation for the various specimens are shown in Figure 6.

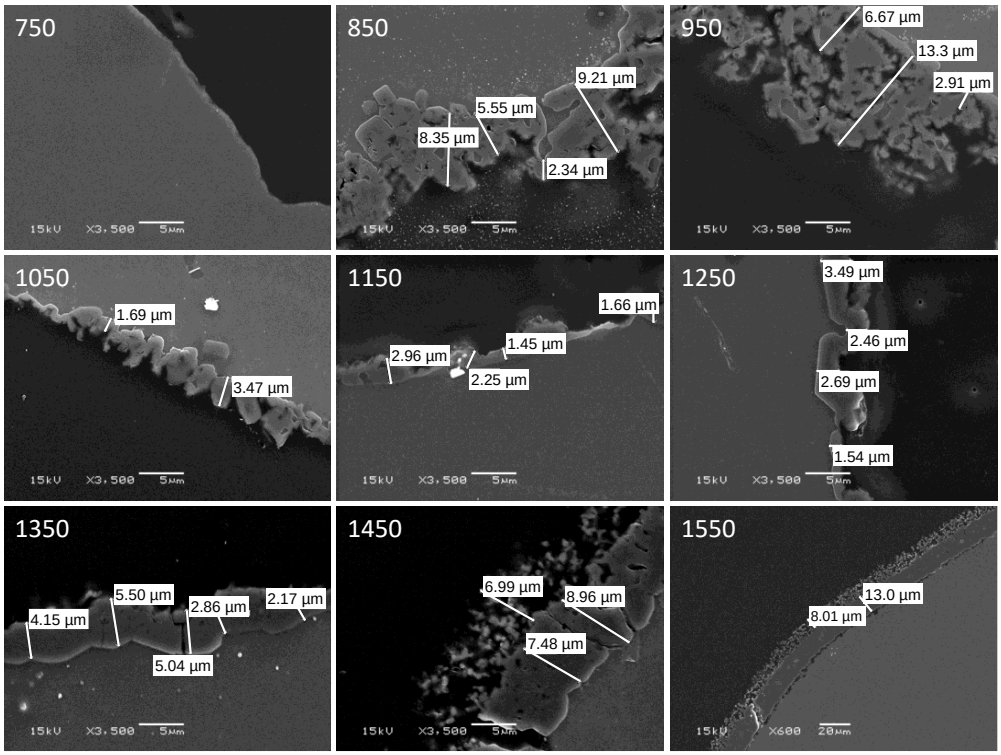



**Figure 6.** SEM images of cross sections of aluminum specimens after oxidation in air at the indicated temperature (°C). Note that all images are shown at the same magnification (scale bar = 5 µm), except for that of the specimen oxidized at 1550 °C (scale bar = 20 µm).

The non-linear variation with oxidation temperature of alumina shell thickness is apparent, as is the change in shell morphology with temperature. Based upon the images, an estimate was made of the thickness of the alumina shell for each specimen, and the results are plotted in Figure 7. Additionally, in Figure 7 are the total mass increases upon oxidation recorded by TGA for the various specimens. The qualitative agreement between the two sets of data is quite good, despite the large uncertainties associated with estimating the thickness of such irregular shell structures.

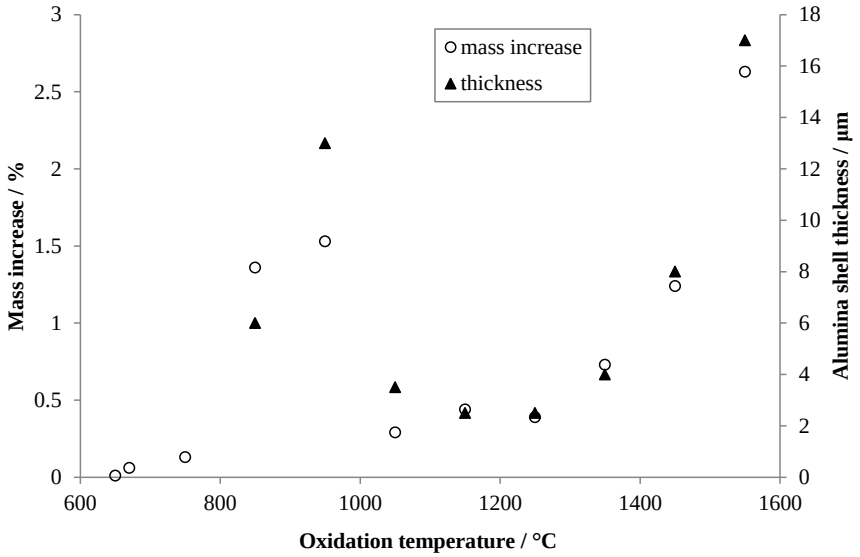



**Figure 7.** Thicknesses of the alumina shells estimated from the images shown in Figure 6 (filled triangles), and total mass gain during oxidation for each specimen recorded by TGA (open circles). Arbitrary scaling has been applied to both y-axes to visually align the two data sets.

Despite the fact that all of the specimens shown in Figure 6 were oxidized at a temperature above the melting point of aluminum, only those heated to 1050 °C or higher formed into spheroidal droplets. The specimens oxidized at 950 °C or below each retained the overall shape of the initial aluminum sheet, presumably due to the stabilizing nature of the native oxide layer which resists fragmentation at the lower temperatures. These samples came out of the TGA/DSC the same shape as they were beforehand (flat sheet), whereas the higher temperature treated samples all converted to spheroidal particles At the higher temperatures reorganization of the alumina shell does occur; this may be a function of increasing flexibility of the alumina with temperature, expansion of the molten aluminum core, increased vapor pressure of aluminum causing fragmentation of the shell, and/or recrystallization of the alumina at higher temperatures allowing facile restructuring of the shell architecture. Additionally, the morphology of the alumina shell changes phase within the temperature range investigated in this study. Between 700 °C and 1050 °C, the morphology of alumina exists in the polycrystalline θ phase with a Face Centered Cubic (FCC) lattice structure. At temperatures above 1050 °C, alumina forms the α phase and takes a Hexagonal Close Packed (HCP) lattice structure.

The outer surface of the alumina shell of a non-sectioned aluminum/alumina sphere produced by oxidizing aluminum sheet at 1050 °C for 12 h was imaged in the SEM, and representative images are shown in Figure 8.

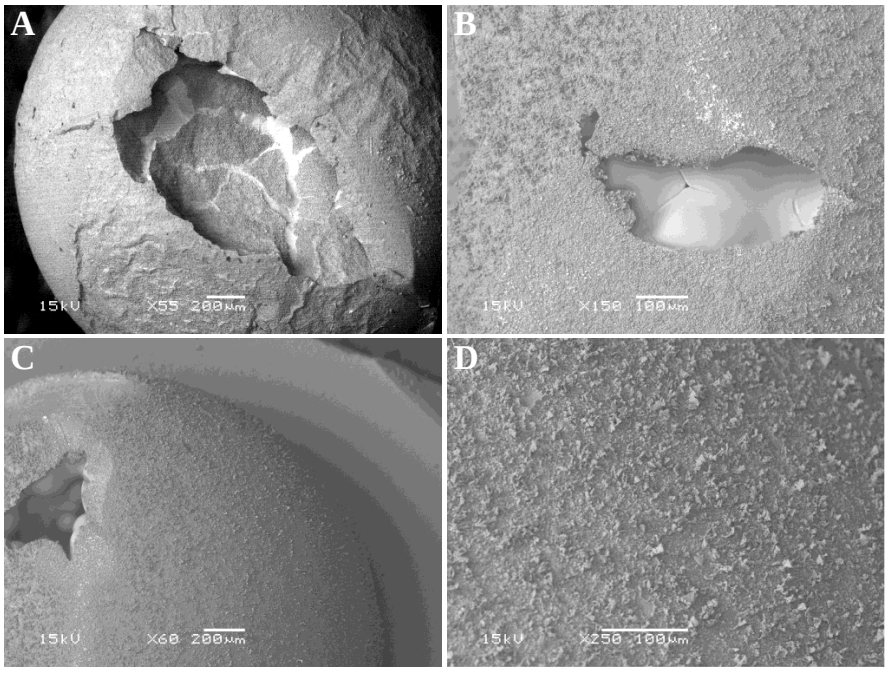



**Figure 8.** SEM images the outer surface of an aluminum specimen after oxidation in air at 1050 °C for 12 h. (**A**,**C**) show the spheroidal nature of the specimens after thermal analysis. (**B**) indicates the presence of grain boundaries in the underlying Al-rich zone. (**D**) shows detail of the surface of a spheroidal particle.

Figure 8A,C show the spheroidal nature of the specimen and areas where the alumina shell collapsed (presumably upon cooling, due to differences in thermal expansion coefficients for aluminum versus alumina). Chemical analysis in the SEM using energy dispersive spectroscopy indicated that the outer surface was alumina (rich in both aluminum and oxygen), while the exposed interior of the sphere was rich in aluminum but contained less oxygen. Figure 8B shows what looks like grain boundaries in the internal Al-rich zone, suggesting that crystallization of the molten aluminum into discrete crystallites occurred upon cooling. Figure 8D shows a close-up of the surface texture, and it appears that dendritic-type growth of alumina occurred on top of a smoother initial coating of alumina on the aluminum particle.

The formation of partially hollow alumina spheres during oxidation of micron-sized aluminum particles has been documented [6] and forms the basis for certain enhanced anti-corrosion coating technologies.

## 4. Conclusions

From the isothermal oxidation experiments described in this paper, several observations can be made:

- The rate or extent of oxidation in air was found to be a non-linear function of the temperature. Different temperature ranges resulted in different behavior, in agreement with the literature.
- At temperatures between 650 °C and 750 °C, very little oxidation took place, even after 12 h exposure to air. At 850 °C oxidation occurred after an induction period, while at 950 °C a similar amount of oxidation occurred as at 850 °C, but more promptly.
- Raising the temperature further resulted in rapid passivation of the surface of the aluminum sheet, as only small and gradual mass increases were measured at oxidation temperatures of 1050 °C, 1150 °C, and 1250 °C. Although the amounts of oxidation occurring at these three temperatures were very small, it was observed that the rates of mass increase was proportionally to temperature.
- At 1250 °C and above, an initial extremely rapid mass increase was observed followed by a more gradual increase in mass. The initial rapid increase was accompanied by a significant exotherm as measured by DSC.
- At temperatures of 1350 °C and above, mass loss was recorded during the temperature ramp under inert atmosphere; the mass loss began at about 1350 °C and became significant above 1400 °C. This is attributed to vaporization of aluminum.
- By scanning electron microscopy (SEM); the observed alumina skin thicknesses correlated qualitatively with the observed mass increases for each oxidation temperature studied. The outer surface of a spheroidal particle produced by oxidation of an aluminum specimen at 1050 °C revealed a partially hollow sphere of aluminum, with a fractured outer alumina shell.
- Specimens oxidized at temperatures below 1050 °C did not transform into spheroidal particles, rather they retained the overall morphology of the aluminum material, presumably due to the stabilizing effect of the native alumina shell at these temperatures.

Since the oxide shell inhibits the hot internal aluminum vapor from comingling with the external oxidizing atmosphere, the shell thickness and quality will influence aluminum particle ignition conditions; this conjecture may address the difficulty which has been experienced in modeling ignition.

**Author Contributions:** Conceptualization, E.N.C., B.D., W.G., N.Y. and F.M.V.; Data curation, N.Y. and F.M.V.; Funding acquisition, E.N.C. and W.G.; Writing—review and editing, E.N.C., B.D., W.G., N.Y. and F.M.V. All authors have read and agreed to the published version of the manuscript.

**Funding:** This research received no external funding.

**Institutional Review Board Statement:** Not applicable.

**Informed Consent Statement:** Not applicable.

**Data Availability Statement:** Not applicable.

**Acknowledgments:** Sandia National Laboratories is a multi-mission laboratory managed and operated by National Technology and Engineering Solutions of Sandia, LLC., a wholly owned subsidiary of Honeywell International, Inc. (Charlotte, NC, USA), for the U.S. Department of Energy's National Nuclear Security Administration under contract DE-NA0003525. Los Alamos National Laboratory is operated by Triad National Security, LLC, for the National Nuclear Security Administration of U.S. Department of Energy (Contract No. 89233218CNA000001).

**Conflicts of Interest:** The authors declare no conflict of interest.

## References


1. Yilmaz, N. Modeling of aluminum particle ignition behavior in open atmosphere rocket propellant fires. *Proc. Inst. Mech. Eng. Part G J. Aerosp. Eng.* **2016**, *230*, 690–697. [CrossRef]
2. Griego, C.; Yilmaz, N.; Atmanli, A. Analysis of aluminum particle combustion in a downward burning solid rocket propellant. *Fuel* **2019**, *237*, 405–412. [CrossRef]
3. Griego, C.; Yilmaz, N.; Atmanli, A. Sensitivity analysis and uncertainty quantification on aluminum particle combustion for an upward burning solid rocket propellant. *Fuel* **2019**, *237*, 1177–1185. [CrossRef]
4. Abernathy, R.N. *Titan 34D-9 abort Cloud Measurements-Quantitative Imagery from Two Camera Sites*; Space and Missile Systems Center Air Force Materiel Command: El Segundo, CA, USA, 1998.
5. Trunov, M.A.; Schoenitz, M.; Dreizin, E.L. Effect of polymorphic phase transformations in alumina layer on ignition of aluminum particles. *Combust. Theory Model.* **2006**, *10*, 603–623. [CrossRef]
6. Kolarik, V.; del Mar Juez-Lorenzo, M.; Fietzek, H. Oxidation of micro-sized spherical aluminum particles. *Mater. Sci. Forum* **2011**, *696*, 290–295. [CrossRef]
7. Yilmaz, N.; Vigil, F.M.; Tolendino, G.; Gill, W.; Donaldson, A.B. Effect of oxide layer formation on deformation of aluminum alloys under fire conditions. *Proc. Inst. Mech. Eng. Part L J. Mater. Des. Appl.* **2016**, *230*, 879–887. [CrossRef]
8. Yilmaz, N.; Vigil, F.M.; Vigil, M.S.; Branam, R.; Tolendino, G.; Gill, W.; Donaldson, A.B. Effect of grain orientation on aluminum relocation at incipient melt conditions. *Mech. Mater.* **2015**, *88*, 44–49. [CrossRef]
9. Jeurgens, L.P.H.; Sloof, W.G.; Tichelaar, F.D.; Mittemeijer, E.J. Growth kinetics and mechanisms of aluminum oxide films formed by thermal oxidation of aluminum. *J. Appl. Phys.* **2002**, *92*, 1649–1656. [CrossRef]
10. Jeurgens, L.P.H.; Sloof, W.G.; Tichelaar, F.D.; Mittemeijer, E.J. Thermodynamic stability of amorphous oxide films on metals: Application to aluminum oxide films on aluminum substrates. *Phys. Rev. B* **2000**, *62*, 4707–4719. [CrossRef]
11. Jeurgens, L.P.H.; Sloof, W.G.; Tichelaar, F.D.; Mittemeijer, E.J. Structure and morphology of aluminum-oxide films formed by thermal oxidation of aluminum. *Thin Solid Film.* **2002**, *418*, 89–101. [CrossRef]
12. Levin, I.; Brandon, D. Metastable alumina polymorphs: Crystal structures and transitions sequences. *J. Am. Ceram. Soc.* **1998**, *81*, 1995–2012. [CrossRef]
13. Dwivedi, R.K.; Gowda, G. Thermal stability of aluminum oxides prepared from gel. *J. Mater. Sci. Lett.* **1985**, *4*, 331–343. [CrossRef]
14. Riano, O.A.; Wadsworth, J.; Sherby, O.D. Deformation of fine-grained alumina by grain boundary sliding accommodated by slip. *Acta Mater.* **2003**, *51*, 3617–3634. [CrossRef]
15. Sibota, N.N.; Shokhina, G.N. Kinetics of polymorphous transformations of anodic alumina. *Kristall und Technik* **1974**, *9*, 913–919.
16. Bergsmark, E.; Simensen, C.J.; Kofstad, P. The oxidation of molten aluminum. *Mater. Sci. Eng. A* **1989**, *120–121*, 91–95. [CrossRef]
17. Jinsong, L.; Ligong, Z.; Haigui, Y.; Nan, Z.; Yongfu, Z.; Xingyuan, L.; Qing, J. Oxidation kinetics of nanocrystalline Al thin films. *Anti-Corros. Methods Mater.* **2019**, *66*, 638–643.
18. Pang, X.; Li, S.; Qin, L.; Pei, Y.; Gong, S. Effect of trace Ce on high-temperature oxidation behavior of an Al-Si-coated Ni-based single crystal superalloy. *J. Iron Steel Res. Int.* **2019**, *26*, 83–87. [CrossRef]
19. Xu, Y.; Liang, W.; Miao, Q.; Jiang, Q.; Ren, B.; Yao, Z.; Zhang, P.; Wei, D. High temperature oxidation behavior of $Al_2O_3$/Al composite coating on $\gamma$ –TiAl. *Surf. Eng.* **2014**, *31*, 354–360. [CrossRef]
20. Novak, P.; Nova, K. Oxidation behavior of Fe-AL, Fe-Si and Fe-Al-Si intermetallics. *Materials* **2019**, *12*, 1748. [CrossRef] [PubMed]
21. Guo, Q.; Chen, J.; Li, J.; Guo, Y.; Yang, Z.; Yang, W.; Xu, D.; Yang, B. Oxidation mechanism of Al-Sn bearing alloys. *Materials* **2021**, *14*, 4845. [CrossRef] [PubMed]


**Disclaimer/Publisher's Note:** The statements, opinions and data contained in all publications are solely those of the individual author(s) and contributor(s) and not of MDPI and/or the editor(s). MDPI and/or the editor(s) disclaim responsibility for any injury to people or property resulting from any ideas, methods, instructions or products referred to in the content.